JGR Oceans

RESEARCH ARTICLE
10.1029/2022JC019326

Key Points:

- Coastal upwelling induced acidification accompanied by oxygen consumption in surface water was observed for the first time in the Pearl River estuary
- Different stoichiometry of oxygen to carbon under influence of upwelling and down-welling favorable winds were observed

Correspondence to:

X. Guo,
xhguo@xmu.edu.cn

Citation:

Guo, X., Su, J., Guo, L., Liu, Z., Yang, W., Li, Y., et al. (2023). Coupling of carbon and oxygen in the Pearl River plume in summer: Upwelling, hypoxia, reoxygenation and enhanced acidification. *Journal of Geophysical Research: Oceans*, *128*, e2022JC019326. https://doi.org/10.1029/2022JC019326

Received 24 SEP 2022
Accepted 31 JUL 2023

Author Contributions:

Funding acquisition: Minhan Dai
Investigation: Jianzhong Su, Liguo Guo, Zhiqiang Liu, Wei Yang, Yan Li, Zhentong Yao, Lifang Wang
Project Administration: Minhan Dai
Resources: Zhiqiang Liu
Supervision: Xianghui Guo, Minhan Dai
Visualization: Wei Yang
Writing – original draft: Xianghui Guo

Coupling of Carbon and Oxygen in the Pearl River Plume in Summer: Upwelling, Hypoxia, Reoxygenation and Enhanced Acidification

Xianghui Guo[1,2], Jianzhong Su[1], Liguo Guo[1], Zhiqiang Liu[3], Wei Yang[1,4], Yan Li[1], Zhentong Yao[1,5], Lifang Wang[1], and Minhan Dai[1]

[1]State Key Laboratory of Marine Environmental Science, College of Ocean and Earth Sciences, Xiamen University, Xiamen, China, [2]Fujian Provincial Key Laboratory for Coastal Ecology and Environmental Studies, Xiamen University, Xiamen, China, [3]Department of Ocean Science and Engineering, Southern University of Science and Technology, Shenzhen, China, [4]College of Harbour and Coastal Engineering, Polar and Marine Research Institute, Jimei University, Xiamen, China, [5]National Marine Environmental Monitoring Center, Dalian, China

Abstract Acidification and hypoxia are universal environmental issues in coastal seas, especially in large river estuaries such as the Pearl River estuary. In July and August of 2015, two legs of a field survey were conducted in the Pearl River plume. Leg 1 was sampled during the influence of upwelling favorable winds, while Leg 2 was during downwelling favorable winds. During both legs, instead of the typically observed dissolved inorganic carbon (DIC) consumption and dissolved oxygen (DO) over-saturation, upwelling-induced high DIC (>2,000 μmol kg^{-1}), low pH (7.7–7.8) and low DO (140–150 μmol kg^{-1}) values were observed in surface waters at the estuary mouth and the area off Hong Kong. In the bottom waters, hypoxia, acidification (pH 7.6–7.8) and DIC accumulation (DIC addition of ∼100–180 μmol kg^{-1}) were observed. Hypoxia was less severe during Leg 2 compared to Leg 1. The stoichiometry of oxygen depletion to DIC addition was 0.89 for bottom water, suggesting remineralization was dominated by marine sourced organic matter. However, a comparison of data from the two legs showed that the stoichiometry of oxygen consumption to DIC accumulation was significantly higher during Leg 2 (0.73 ± 0.03 for Leg 1 vs. 0.80 ± 0.05 for Leg 2), although N/P ratios were the same (13.54 ± 1.93 for Leg 1 vs. 13.51 ± 2.04 for Leg 2). This phenomenon was attributed mainly to enhanced ventilation (re-oxygenation) under the influence of the downwelling favorable winds during Leg 2. Although ventilation relieves some hypoxia, it might enhance acidification in bottom waters after a short-term ventilation event. The enhanced acidification after short-term ventilation is worthy of further study considering that most hypoxia and acidification are found in shallow coastal seas.

Plain Language Summary Acidification and hypoxia are universal environmental issues in coastal seas. In the summer of 2015, we conducted two survey legs in the Pearl River plume of the northern South China Sea. Legs 1 and 2 were conducted under the influence of upwelling favorable and downwelling favorable winds, respectively. During both legs, upwelling induced subsurface water characterized by high dissolved inorganic carbon (DIC), low pH and low dissolved oxygen to the sea surface of the coastal area. In the bottom waters, hypoxia, acidification and DIC accumulation were observed. Hypoxia was less severe during Leg 2 compared to Leg 1. Comparison between the two legs showed that the stoichiometry of oxygen consumption to DIC accumulation was significantly higher during Leg 2, which was attributed mainly to the enhanced ventilation under the influence of the downwelling favorable winds. Although ventilation relieves hypoxia, it might enhance acidification after short-term ventilation. This phenomenon should get more attention as most hypoxia and acidification are observed in shallow coastal areas.

1. Introduction

Hypoxia has become a universal environmental and ecological problem in recent decades (Caballero-Alfonso et al., 2015; Carstensen et al., 2014; Feely et al., 2018; Fennel & Testa, 2019; Rabalais et al., 2010). In the northern Gulf of Mexico and the East China Sea influenced by large rivers, seasonal hypoxia in shallow bottom water occurs in summer, due mainly to the combination of microbial remineralization and hydrodynamic mechanisms (Li et al., 2002; Rabalais et al., 2002, 2010; Wang et al., 2016). Eutrophication in the coastal ocean stimulates primary production, forming increased amounts of marine organic matter that subsequently fuels dissolved oxygen (DO) consumption in bottom waters (Carstensen et al., 2014; Rabalais et al., 2010; Y. Y. Zhao

et al., 2020). In addition to driving the formation of hypoxia, eutrophication-enhanced primary production eventually worsens coastal ocean acidification, as reported in the northern Gulf of Mexico, the East China Sea, the Namibian coast, the Oregon shelf, the St. Lawrence estuary and the adjacent Scotian shelf (Cai et al., 2011; Chou et al., 2013; Fennel & Testa, 2019; Grantham et al., 2004; Jiang et al., 2019; Jutras et al., 2020; Monteiro et al., 2006). Coastal upwelling is also an important process that brings acidified subsurface or bottom waters to the sea surface, as observed in the waters off California (Feely et al., 2008). On the northern South China Sea shelf and in the upwelling zone near Hai'nan Island, intensified coastal upwelling in summer brings low pH water to the sea surface (Cao et al., 2011; Dong et al., 2017; Gan et al., 2009; Jing et al., 2015; P. G. Lin et al., 2016). However, field observations of upwelling's influence on surface water in the large river estuaries are few.

Summer bottom water hypoxia and acidification are usually observed in shallow coastal seas (Li et al., 2002; Rabalais et al., 2010; Y. Y. Zhao et al., 2021). Episodic ventilation events, such as perturbations induced by typhoons, hurricanes, storms, or local strong wind events might temporarily relieve the hypoxia (X. P. Hu et al., 2017; Y. Y. Zhao et al., 2021); however, as the equilibration time of CO_2 is ~10-fold slower than for O_2 (Zeebe & Wolf-Gladrow, 2003), these episodic reoxygenation events may enhance acidification in bottom water by supplying it with oxygen and enhancing the aerobic respiration of organic matter, while the dissolved inorganic carbon (DIC) change is much smaller (X. P. Hu et al., 2017). Subsequently, the acidification of the hypoxic bottom water might become more severe than it was before the perturbation. However, field observations of reoxygenation-enhanced ocean acidification in bottom water are very difficult to achieve.

The Pearl River estuary is a large river estuary-shallow shelf system perturbed by extensive human activities in the northern South China Sea. There are two hypoxic zones in the Pearl River estuary/plume: one in the upper estuary near the mega-city Guangzhou, where year-round hypoxia was observed in the entire water column from 2000 to 2005 (Dai et al., 2006; Guo et al., 2009; Zhai et al., 2005), and the second in bottom waters of the lower estuary, which occurs mainly in summer. The latter hypoxic area, which this study focuses on, appeared occasionally in the 1980s and 1990s and became more frequent after 2010 (H. Y. Lin et al., 2001; Qian et al., 2018; Yin et al., 2004). On the northern South China Sea shelf, interactions between the Pearl River plume and east Guangdong coastal upwelling increase the complexity of quantifying the underlying biogeochemical processes (Cao et al., 2011; Han et al., 2012). Although these interactions between the plume and coastal upwelling on the northeastern South China Sea shelf are well-known, observations of low DO and acidified surface waters induced by upwelling near the Pearl River estuary mouth have not been reported. In this study, we report for the first time surface waters with upwelling-induced low DO and acidification in the lower Pearl River estuary in summer based on field observations. Hypoxia and acidification in bottom waters are also addressed. Furthermore, enhanced acidification after short-term ventilation, which is very difficult to capture in field observations, is discussed.

2. Materials and Methods

2.1. Study Area and Cruise Background

The Pearl River is the second largest river in China and the thirteenth largest river in the world in terms of freshwater discharge, with an annual discharge of 3.26×10^{11} m^3 (Dai et al., 2014; H. T. Zhao, 1990). About 80% of the freshwater discharge occurs in the wet season from April to October, driven by the Asian monsoon (Dai et al., 2014; H. T. Zhao, 1990). The Pearl River system has three main tributaries, namely the West River, the North River and the East River, as well as several local rivers in the delta. All runoff from the Pearl River system discharges into the northern South China Sea through eight major outlets via three sub-estuaries: the Lingdingyang, Modaomen, and Huangmaohai (Figure 1).

The Pearl River estuary is located in a sub-tropical climate zone. The freshwater from the Pearl River system forms the Pearl River plume. Generally, it flows southwestwardly under the influence of the northeast monsoon in the cold season and northeastwardly under the influence of the southwest monsoon in the warm season (J. Y. Hu et al., 2000). The lower Pearl River estuary and plume are stratified in the warm season, with high primary production in surface waters, while low DO or even hypoxia occurs in the bottom water, due mainly to remineralization of marine sourced organic matter (Su et al., 2017).

With the support of the CHOICE-C II project (Carbon cycling in China Seas-budget, controls and ocean acidification II), a field survey was conducted in the Pearl River plume from July 18 to August 8, 2015 onboard the R/V

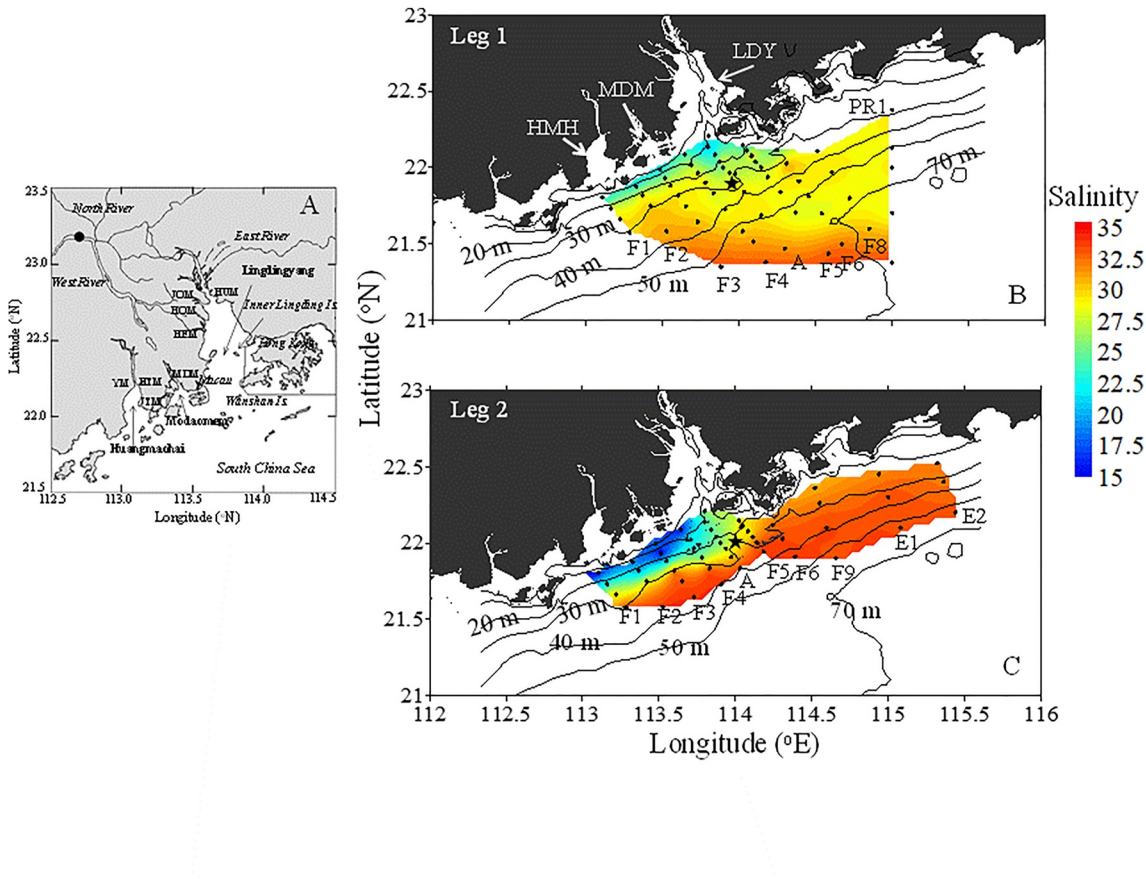

Figure 1. Map of the Pearl River estuary and plume with sampling stations. In panel (a), the solid black circle is the location of the Wuzhou gauge station; the eight main outlets Humen (HUM), Jiaomen (JOM), Hongqimen (HQM), Hengmen (HEM), Modaomen (MDM), Jitimen (JTM), Hutiaomen (HTM), Yamen (YM) are also marked. In panels (b) and (c), LDY (Lingdingyang), MDM (Modaomen) and HMH (Huangmaohai) are the three sub-estuaries of the Pearl River estuary. F1-F9, PR1, and E1-E2 are the transects conducted during the surveys. Isobaths of 20–70 m are also marked. The star marks the location of the buoy. The sea surface salinity distributions show the different orientations of the river plume during the two legs of the survey.

Haidiao 6. The cruise included two legs: Leg 1 was conducted from July 18 to 31 and Leg 2 was conducted from August 1 to 7 (Figure 1). No typhoon or tropical storm passed through the Pearl River plume during the cruise.

The freshwater discharge from the Pearl River is highest in summer (Figure 2). In 2015, the monthly average freshwater discharge of the West, North, and East Rivers in July were similar to the long-term monthly average, suggesting that the study area was under the influence of the general summer discharge during the survey period (Figures 2a and 2b).

2.2. Sampling and Analysis

We repeated the measurements along 9–10 transects orientated in the cross-shelf direction during each leg of the cruise. At each station, depth profiles of salinity and temperature were recorded with a Seabird® SBE 917 Conductivity-Temperature-Depth/pressure (CTD) sensor package. Discrete water samples were collected at selected stations with 12-L Niskin bottles mounted on a Rosette sampler.

Sub-samples for DO, pH, DIC and total alkalinity (TA) were taken with Tygon® tubing free of air bubbles, with ample sample overflow in order to minimize any contamination from atmospheric O_2 or CO_2. Samples for DO were sampled with 60 mL biological oxygen demand bottles and fixed with Winkler reagents (Carpenter, 1965). Samples for pH were taken into 120 mL amber glass bottles and poisoned with 100 μL of a saturated $HgCl_2$ solution. Samples for DIC/TA measurements were taken in 250 mL borosilicate bottles with ground glass stoppers and poisoned with 200 μL of the saturated $HgCl_2$ solution. Samples for nutrient measurement were filtered with 0.45 μm polyacetate filters and measured onboard.

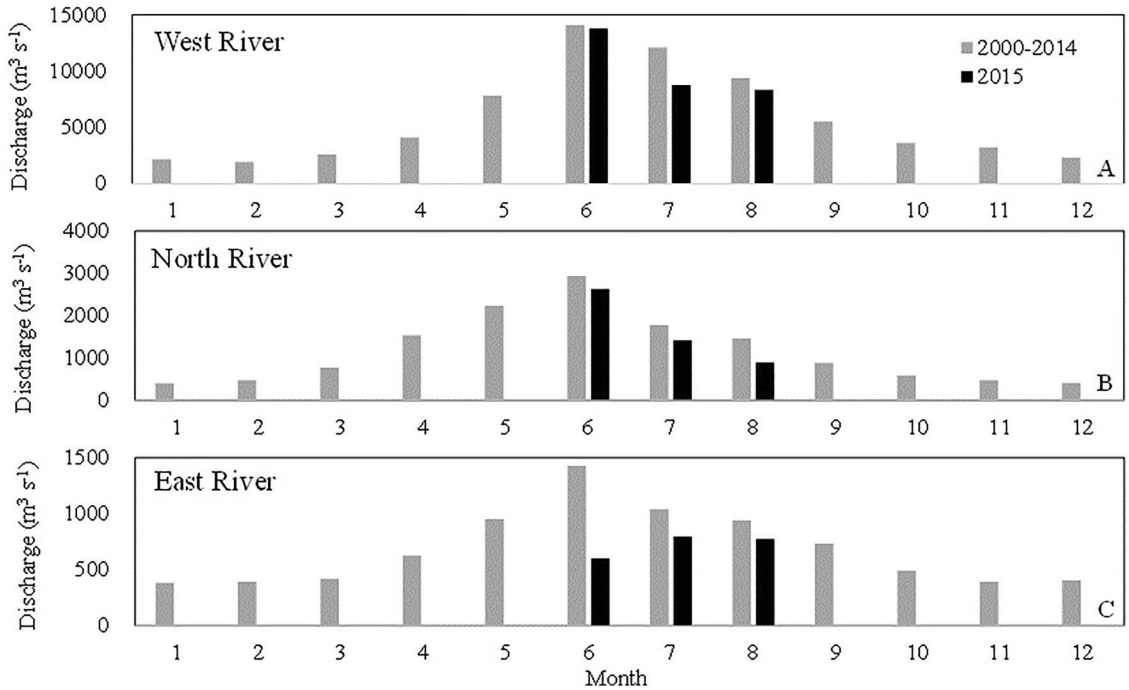

Figure 2. Freshwater discharges of the three main tributaries (the West River, North River, and East River) of the Pearl River. Data are from Water Resources Bureau and Pearl River Water Resource Commission of the Ministry of Water Resources (http://xxfb.hydroinfo.gov.cn/; http://swj.pearlwater.gov.cn/syqxx/index.shtml).

DO samples were measured spectrophotometrically at 466 nm onboard within 4 hr of sampling (Labasque et al., 2004). The samples were placed in a thermostatic bath at 25.00 ± 0.01°C for about 1 hr before measurement. pH samples were measured onboard within 2 hr of sampling with an Orion 3 Star pH meter and an Orion VR8102BN Ross combination electrode calibrated against Tris and AMP buffers (Dickson et al., 2007). Samples for pH measurements and buffers were placed in a thermostatic bath at 25.00 ± 0.01°C for about 1 hr before measurement; therefore, the pH values are given at 25°C on the total scale.

The DIC/TA samples were stored in the dark at room temperature and returned to the land-based laboratory at Xiamen University for analysis, which was conducted within 1 month. Analyses of DIC and TA followed the methods of Cai et al. (2004). DIC was measured by collecting and quantifying the CO_2 released from the sample upon acidification with a non-dispersive infrared detector (Li-Cor® 7,000) using an Apollo SciTech model AS-C3 DIC Analyzer with a precision of ±2 μmol kg^{-1}. TA was determined by Gran titration using an automated alkalinity titrator (Apollo SciTech model AS-ALK1+) with a precision of ±2 μmol kg^{-1}. Both DIC and TA were calibrated with the certified reference materials (CRM) provided by Dr. A. G. Dickson of the Scripps Institution of Oceanography to achieve an accuracy of ±2 μmol kg^{-1}.

Nutrient samples were measured with an AA3 Auto-Analyzer (Bran-Lube, GmbH). Nitrate plus nitrite (N+N) was determined using copper-cadmium column reduction and the pink azo dye method (Hansen & Koroleff, 1999). Soluble reactive phosphorus (SRP) was determined by the phosphomolybdenum blue method (Hansen & Koroleff, 1999). The detection limits for N+N and SRP were 0.1 and 0.08 μmol L^{-1}, respectively, and the analytical precision was 1% for N+N and 2% for SRP (Han et al., 2012).

Wind speed and direction were measured with a Yong 05106 marine wind sensor at ~10 m above the sea surface on a buoy, which was located in the middle of the study area (black star in Figure 1), which is also the center of the bottom hypoxic area. The precisions of wind speed and wind direction were ±0.3 m s^{-1} and ±3°, respectively.

2.3. Data Processing

2.3.1. Calculations of DIC_{Excess} and AOU

The DIC and pH values at equilibrium with atmospheric CO_2 (DIC_{Equ} and pH_{Equ}) were calculated using TA and atmospheric partial pressure of CO_2 (pCO_2) with the CO2SYS program (Version 14, Pierrot et al., 2006).

The dissolution constants of carbonic acid are from Millero et al. (2006). The CO_2 solubility coefficient is from Weiss (1974) and the sulfate dissociation constant is from Dickson (1990). The measured SRP and SiO_2 data were used as ancillary input parameters to get more accurate calculated carbonate system parameters as both SRP and SiO_2 contribute alkalinity. 400 μatm was taken as the average atmospheric pCO_2 value.

Excess DIC (DIC_{Excess}) is defined as the difference between the observed DIC and DIC_{Equ} following Xu et al. (2017). Similarly, the pH change due to organic matter remineralization is defined as the difference between the observed pH and the pH_{Equ}. Apparent oxygen utilization (AOU) is defined as the difference between saturated and observed DO concentrations. The saturated oxygen concentration is calculated according to the empirical formula of Garcia and Gordon (1992).

2.3.2. Calculations of Conservative Mixing TA, DIC and pH

We use a three end-member mixing model to simulate the influence of the upwelling on DIC, TA and pH. First, salinity (S) and potential temperature (θ) were adopted as conservative parameters to estimate the fractions of water from the three end-members following Cao et al. (2011) and Han et al. (2012).

$$f = f_E + f_S + f_B \tag{1}$$

$$S = S_E \times f_E + S_S \times f_S + S_B \times f_B \tag{2}$$

$$\theta = \theta_E \times f_E + \theta_S \times f_S + \theta_B \times f_B \tag{3}$$

In the above equations, f is the water fraction; the subscripts "E", "S," and "B" denote estuarine water, surface water, and bottom water, respectively.

Using the above equations, water fractions can be resolved. Subsequently, conservative mixing values for TA (TA_{Con}) and DIC (DIC_{Con}) can be calculated by multiplying the end-member TA and DIC by the water fractions (Equations 4 and 5).

$$TA_{Con} = TA_E \times f_E + TA_{Sur} \times f_{Sur} + TA_{Sub} \times f_{Sub} \tag{4}$$

$$DIC_{Con} = DIC_E \times f_E + DIC_{Sur} \times f_{Sur} + DIC_{Sub} \times f_{Sub} \tag{5}$$

With DIC_{Con} and TA_{Con} as input parameters, conservatively mixed pH values can be calculated using CO2SYS (Version 14, Pierrot et al., 2006). The constants selected are the same as those described in Data processing.

2.3.3. Calculation of Stratification Factor

Stratification factor (n) was calculated following Hansen and Rattray (1966).

$$n = \frac{S_b - S_s}{S_a} \tag{6}$$

In which, S_b, S_s, and S_a are the salinities of the bottom water, surface water, and water column average, respectively.

In this study, all the contours maps presented in this study were made with the software Surfer 8 with Kriging gridding method.

3. Results

3.1. Wind Field and Hydrologic Setting

Figure 3 illustrates the hourly variability of along-shore winds in the Pearl River plume area (at the buoy location in Figure 1). The along-shore wind, according to Liu et al. (2018, 2020) and the orientation of the regional isobaths, is defined as wind blowing 22.8° to the east. A positive value then indicates northeastward upwelling-favorable winds.

The shelf current in July is generally driven by upwelling-favorable winds, which also experience notable synoptic variabilities. Before the cruise, downwelling-favorable northeasterly winds blew over the shelf off the Pearl River estuary from July 5 to 11, and gradually reversed to blow northeastward (upwelling-favorable winds) during July 11 to 18. The shelf current was then forced by a short-period of downwelling-favorable southeasterly

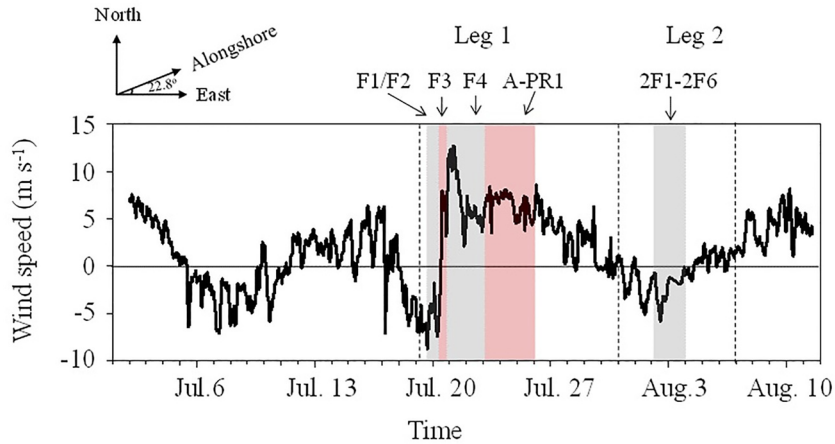

Figure 3. Along-shore wind speed in the Pearl River plume measured from the buoy located in the middle of the study area (star in Figure 1). The positive values indicate upwelling-favorable winds, while negative value are downwelling-favorable winds. The vertical dashed lines indicate the two legs. The letters and numbers mark the timing of visits to transects during the periods (also denoted by the alternating gray and pink shaded regions).

winds on July 18 to 19 at the beginning of the Leg 1 mapping (transects F1 and F2). The predominant winds then rapidly reversed to blow northeastward (upwelling-favorable), and this pattern persisted until decaying at the end of Leg 1. The shelf current was mainly driven by the prevailing downwelling-favorable southeasterly wind during our Leg 2 mapping (August 3–5).

Influenced by the wind field, the orientation of the plume and the hydrologic settings between the two legs differed. During Leg 1, the study area was under the influence of the upwelling-favorable winds, except when the two westernmost transects were visited. Sea surface temperatures (SST) ranged from 26.2 to 30.1°C, with cold waters observed at the estuary mouth and the inshore area east of the estuary (Figure 4a-1). Warm water was observed in the western area, where it was influenced by downwelling-favorable wind when we surveyed (Figure 3). Sea surface salinities (SSS) ranged from 20.6 to 33.9. The plume enveloped by the surface isohaline with SSS<32 was oriented northeastward from the estuary and extended offshore to 21.5°N. The lowest salinity was observed at the estuary mouth (Figure 4b-1). During Leg 2, although the SST range (26.1–30.6°C) was similar to that of Leg 1, the distribution pattern was different. Low SSTs at the estuary mouth were still observable, but the SST of the inshore water east of the estuary increased, suggesting that the upwelling was limited to the estuary mouth (Figure 4a-2). The distribution pattern of SSS during Leg 2 was also different from Leg 1. During Leg 2, the low salinity plume extended southwestward in the coastal waters to the west of the estuary due to the downwelling-favorable wind, and lower SSSs (14.4–33.7) were observed (Figure 4b-2). During Leg 2, the upwelling remained although the upwelling-favorable wind relaxed, which was consistent with the results of the modeling study of Zu and Gan (2015).

At the bottom, temperatures were 20.4–29.5°C during Leg 1, with warmer waters observed at the estuary mouth and along the west coast suggesting influence of the plume. Salinity ranged from 23.1 to 34.6, with fresher waters observed at the estuary mouth and in the coastal area west of the estuary. During Leg 2, the highest temperature in the estuary was 25.9°C and the lowest salinity was 30.1 (Figure 5).

Figure 6 presents the sectional distributions of the parameters along transect A, which is in the center of the sampling region and plume, and includes the buoy observing station. The shoaling isotherm and isohaline in the inshore direction suggested coastal upwelling during both legs (Figure 6). The upwelling induced the relatively low temperatures and high salinities at the estuary mouth (Figures 4 and 6).

3.2. Spatial Distributions of Carbonate Parameters and DO

3.2.1. Surface Water

Generally, the distribution pattern of TA was similar to that of salinity: that is, low TA was found in the low salinity area and high TA was found in the offshore high salinity area, suggesting the dominant influence of water

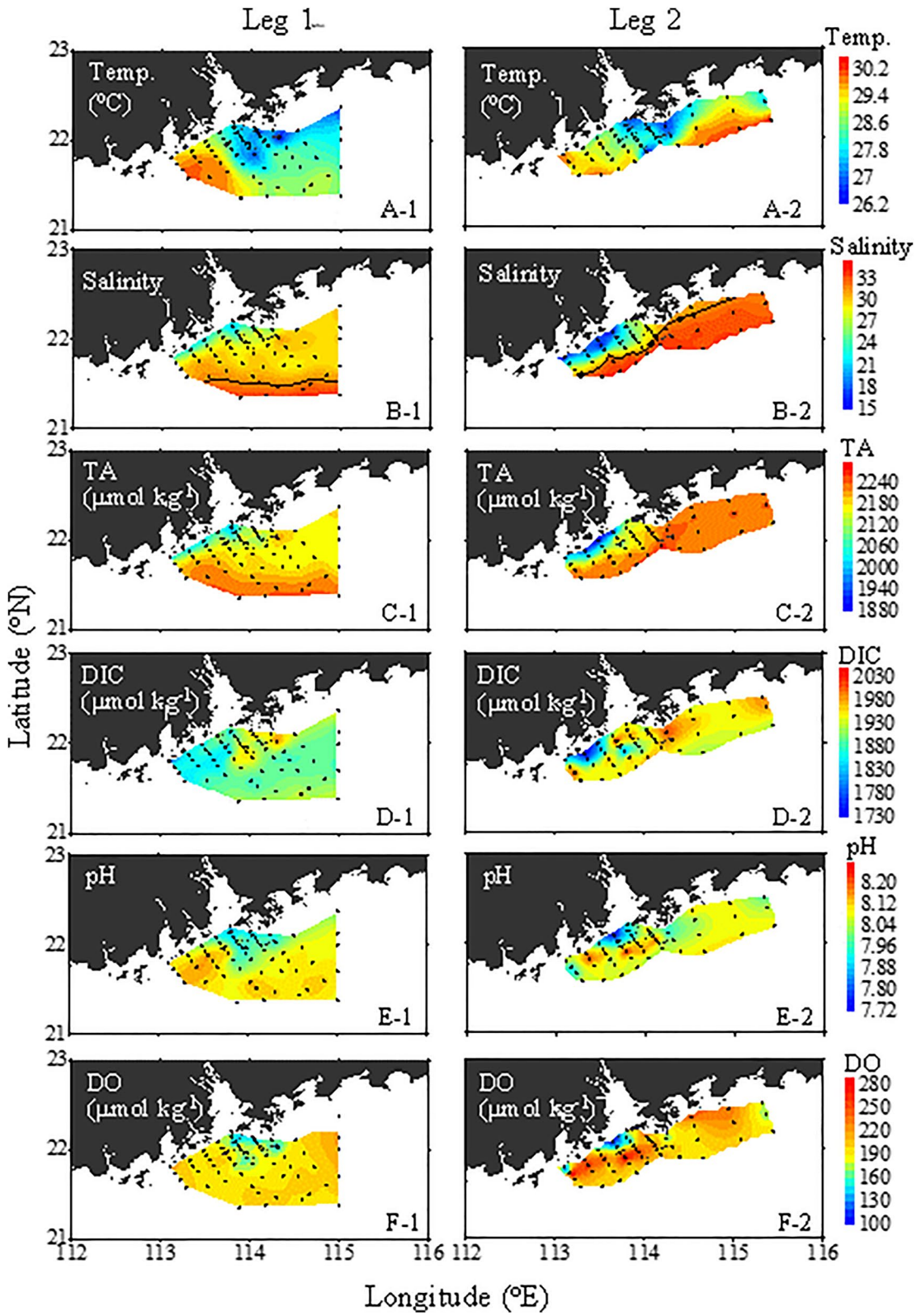

Figure 4. Distributions of temperature (Temp.), salinity, total alkalinity (TA), dissolved inorganic carbon (DIC), pH, and dissolved oxygen (DO) of the surface water. The black dots indicate the sampling stations. Black lines in panels b-1 and b-2 are the isohalines of salinity 32.0.

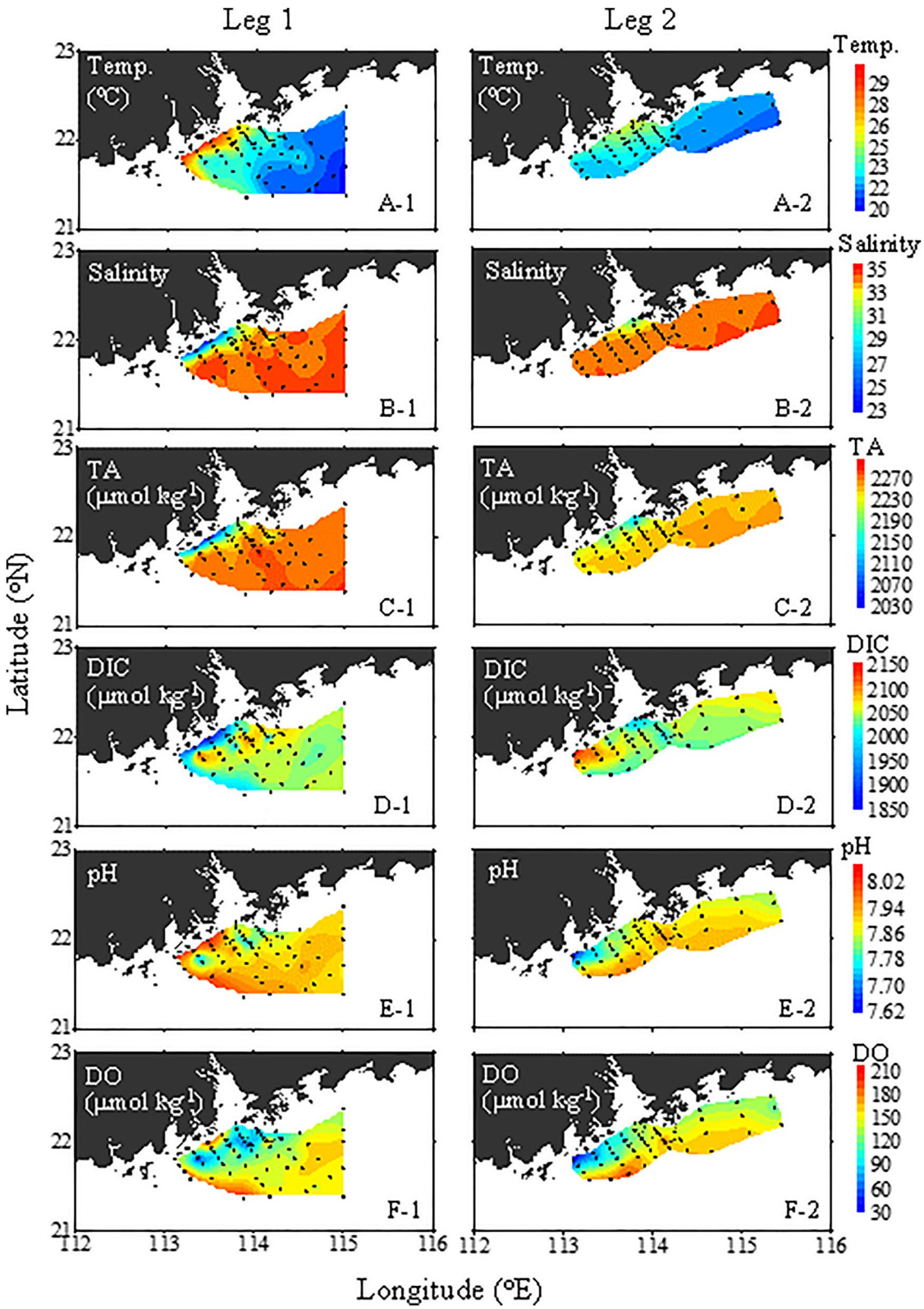

Figure 5. Distributions of temperature (Temp.), salinity, total alkalinity (TA), dissolved inorganic carbon (DIC), pH, and dissolved oxygen (DO) of the bottom water. The black dots indicate the sampling stations.

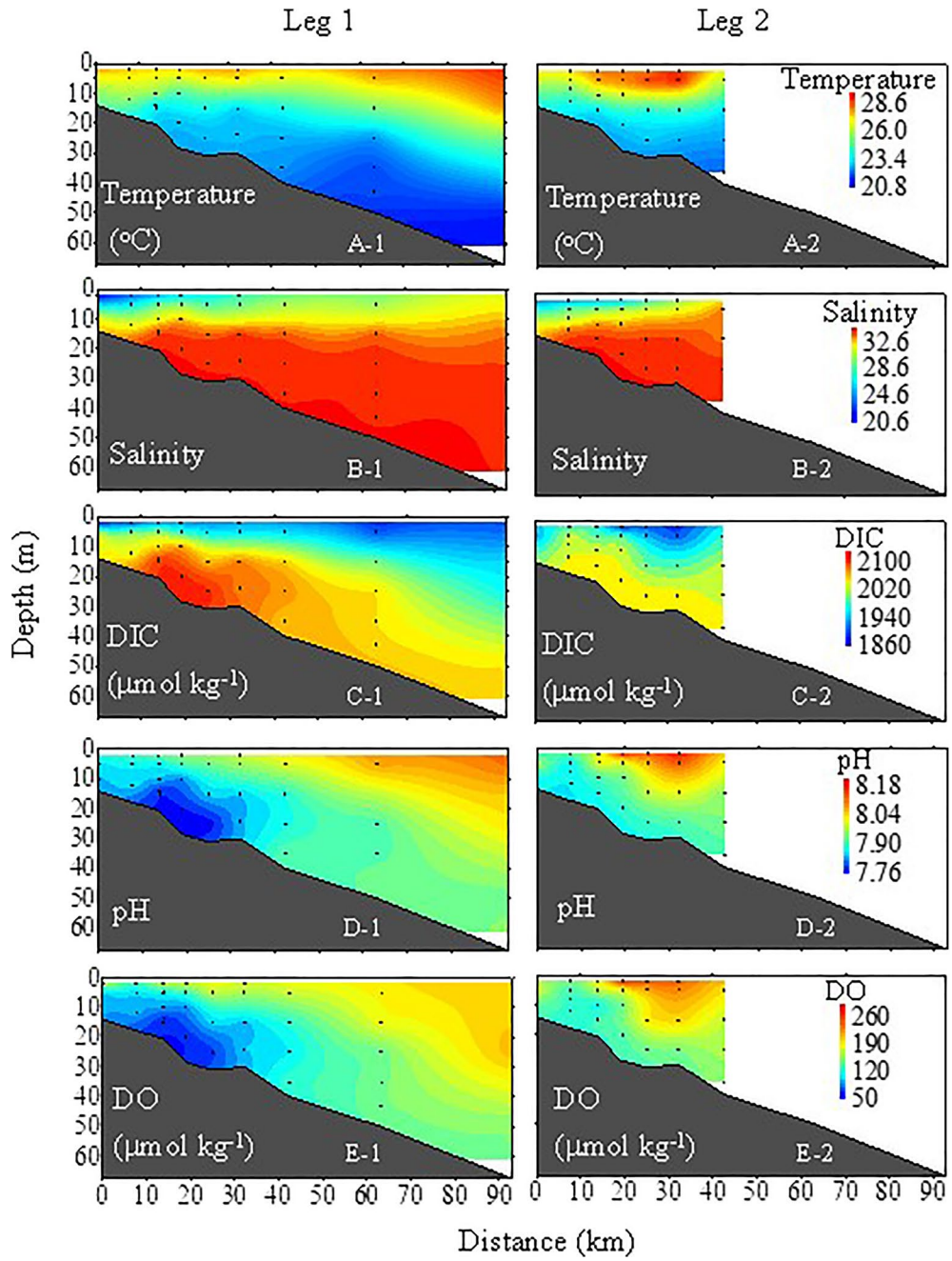

Figure 6. Sectional distributions of temperature (Temp.), salinity, total alkalinity (TA), dissolved inorganic carbon (DIC), pH, and dissolved oxygen (DO) in transect A. The black dots indicate the stations and sampling depths.

mixing on TA distribution (Figures 4c-1 and 4c-2). However, the distribution pattern of DIC was different and generally opposite to that of SST. During both legs, the highest DIC values (>2,000 μmol kg^{-1}) were observed in low SST areas, and lower DIC values were located in low salinity areas (Figures 4d-1 and 4d-2). These DIC distribution patterns suggest the combined influence of the river plume and upwelling. Generally, the bottom water was characterized by high DIC as a result of remineralization of organic carbon, while TA showed minor influence by this process. Therefore, DIC and TA distributions showed apparently different responses to the upwelling.

The pH range was 7.87–8.18 during Leg 1 and 7.73–8.28 during Leg 2 (Figures 4e-1 and 4e-2). During Leg 1, the lowest pH (<7.9) was found in the upwelling center and high values were observed in the offshore area and

the western area. However, low pH values during Leg 2 were found in both the upwelling center and the area of lowest salinity. In addition, there were two high pH patches (8.20–8.27) during Leg 2.

DO ranged from 129 to 238 μmol kg^{-1} (60%–114%) during Leg 1 and 100–314 μmol kg^{-1} (46%–152%) during Leg 2 (Figures 4f-1 and 4f-2). The spatial distribution pattern of DO was similar to that of SST, with the lowest DO observed in the upwelling center and the low salinity estuary mouth. Two high DO patches (up to 130%–152%) during Leg 2 were accompanied by high pH (8.20–8.27) and DIC depletion (Figure 4), suggesting strong photosynthesis.

3.2.2. Bottom Water

The spatial distribution of TA in bottom water also closely followed that of salinity. Low TA was observed in the estuary mouth and northwest coast where salinity was low, and higher TA was found in the offshore area. In most of the study area, TA was lower during Leg 2 than Leg 1.

During Leg 1, although the northwest coast (low salinity area) was characterized by low DIC, the highest DIC was not in the offshore area. Instead, there were several high DIC patches (>2,100 μmol kg^{-1}) at the estuary mouth and in the area off Hong Kong. The distribution pattern of pH was opposite that of DIC, with low pH values (<7.8) in the high DIC patches. The distribution pattern of DO was similar to that of pH, with low DO (<90 μmol kg^{-1}) in the high DIC and low pH patches. During Leg 2, DIC, pH and DO were also strongly coupled. However, in contrast to Leg 1, the high DIC, low pH and low DO area was observed in northwestern corner of the study area. The high DIC, low pH and low DO patches observed during both legs suggest strong organic carbon remineralization (Figure 5).

Comparison between the two legs shows that TA was generally lower during Leg 2 than Leg 1, except along the northwest coast. At the estuary mouth and the area off Hong Kong, DIC was lower, and pH and DO were higher during Leg 2 than Leg 1. In contrast, DIC was higher, and pH and DO were lower at the northwest corner during Leg 2 than Leg 1.

As shown in the sectional distribution of transect A, there was a center of high DIC, low pH and low DO in the bottom water during Leg 1 (Figure 6). However, DIC decreased, but pH and DO increased conspicuously at that location during Leg 2. The distribution patterns of the parameters in transects F4, F5, and F6 (not shown) were similar to those in transect A.

3.3. Water Fractions and Conservative Mixing of Carbonate Parameters

The relationships between θ and DIC with salinity (Figure 7) suggest a three end-member mixing scheme in the study area: fresher Pearl River estuary water (high temperature, low salinity, and low DIC), offshore surface water (high temperature, high salinity, and relatively low DIC) and sub-surface/bottom waters (low temperature, high salinity, and highest DIC).

During Leg 1, estuarine water accounted for an important fraction (40%–100%) in the plume, and surface water accounted for a high ratio (>70%) in the offshore area (Figures 8a-1 and 8b-1). Fraction of bottom water was generally low, but it contributed 20%–40% at the estuary mouth and inshore areas (Figure 8c-1). During Leg 2, the fraction of estuarine water in the western inshore corner was high (up to 80%–100%), but the area was very limited (Figure 8a-2), which was consistent with the smaller plume area during Leg 2. Fraction of surface water accounted for larger area than Leg 1 (Figures 8b-1 and 8b-2). The range of fraction of bottom water during Leg 2 was similar to Leg 1, but only limited to the estuary mouth (Figures 8c-1 and 8c-2).

The calculated results of conservative mixing TA, DIC, and pH for the surface waters are shown in Figure 9. Compared with the observations (Figure 4), the general spatial distribution patterns of the simulated DIC, TA and pH are qualitatively consistent with the observed distribution patterns during both legs (except for the observed patches of high pH and low DIC during Leg 2).

4. Discussion

4.1. Upwelling-Induced High DIC, Low Oxygen and Acidified Surface Water at the Estuary Mouth

The Pearl River plume and the offshore area of Hong Kong are generally characterized by low salinity, low DIC, high pH, and high DO in surface waters (Guo et al., 2009; Y. Y. Zhao et al., 2020). However, during our cruise

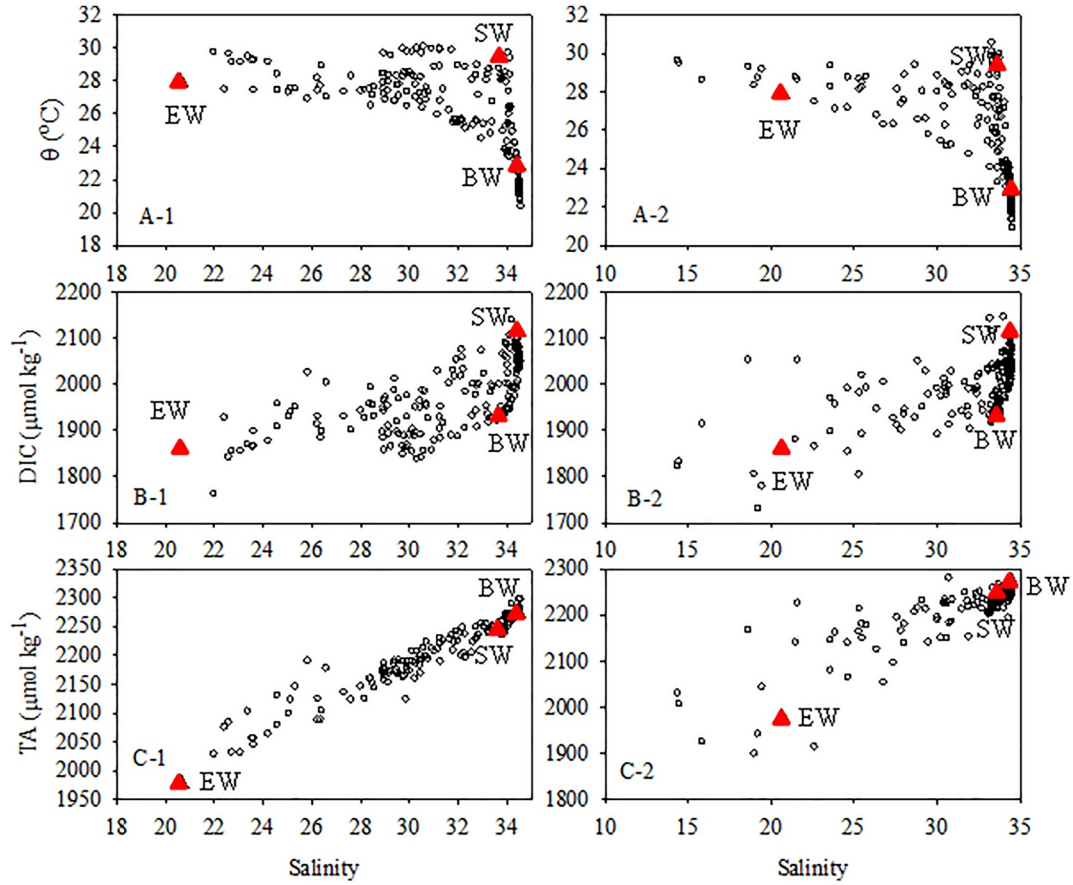

Figure 7. Relationships of potential temperature (θ), dissolved inorganic carbon (DIC) and total alkalinity (TA) with salinity in the water column during the two legs of surveys. The solid triangles indicate the end-member values. a-1, b-1 and c-1 are data from Leg 1; b-2, c-2 and d-2 are data from Leg 2. EW is the estuarine water end-member (surface water of station A10); SW is the surface water end-member (average of the surface water at stations A16 and A7); BW is the bottom water end-member (average of the bottom water at stations A13 and A4).

(especially during Leg 1) DIC was high while pH and DO were low, which has never been reported. Upwelled subsurface or bottom water may drive the observed patterns given that the center of the region contained high DIC and low DO, but low temperatures and high salinities.

Although we used a similar three end-member mixing model in our study, it was different from Su et al. (2017) and Y. Y. Zhao et al. (2020), as "contaminated" local bottom water characterized by high DIC and low DO was adopted as the bottom water end-member to qualitatively demonstrate the influence of the upwelling on the surface water characteristics (Table 1).

The general similar distribution patterns of the conservative mixing of the carbonate system parameters with the observations confirms that upwelling induced the high DIC and acidified surface water at the Pearl River estuary mouth and offshore area of Hong Kong.

In transect F6 in the upwelling center, the average conservative mixing TA values were 2,183.3 ± 36.8 and 2,243.2 ± 8.6 μmol kg^{-1}, respectively, during the two legs, which were very close to the observations, that is, 2,184.4 ± 31.1 μmol kg^{-1} during Leg 1 and 2,242.0 ± 11.3 μmol kg^{-1} during Leg 2. The calculated conservative mixing DIC during the two legs were 1,946.0 ± 29.2 and 1,969.6 ± 34.8 μmol kg^{-1} and they were 19.7 μmol kg^{-1} higher or 9.7 μmol kg^{-1} lower than the observed values (Table 2, the transect south of Hong Kong in Figures 4 and 9). The differences between the calculated conservative mixing DIC and the observations might be attributed to the influences of the air-sea CO_2 exchange and biogeochemical processes.

The consistence of the conservative mixing values with the observations in other transects were not as good as transect F6. Comparison between the two legs, the consistence of the calculated conservative mixing with the

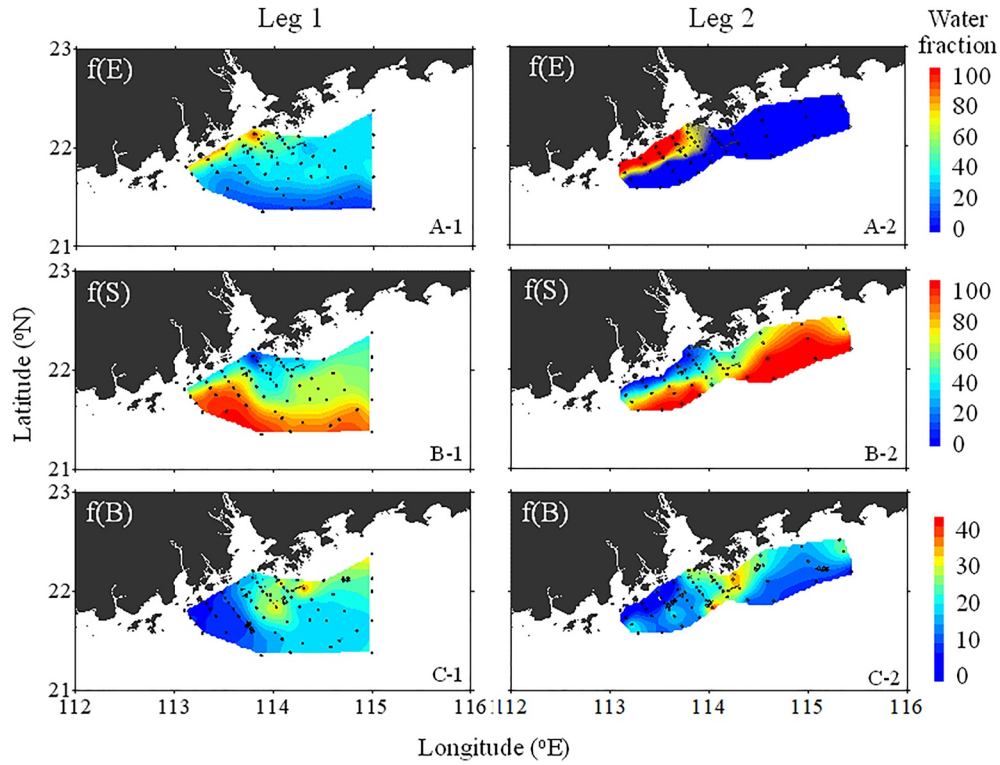

Figure 8. Spatial distributions of water fractions (in %) in the surface water during the two legs of the survey. *f*(E), *f*(S), and *f*(b) denote the fractions of estuarine water, offshore surface water and bottom water end-members, respectively. Note that the color bar of panels (c-1) and (c-2) is different from panels (a-1) to (b-2).

observations was generally better during Leg 1 than Leg 2. This is because the main driver of this difference is biogeochemical processes given the longer equilibration times necessary for CO_2. It was generally rainy or cloudy during the survey of Leg 1 and photosynthesis was thereby depressed. The largest difference was the high pH and high DO patches during Leg 2 (Figures 4e–2 and 9c-2), which were mainly attributed to localized patches of strong photosynthesis, as sometimes the weather during Leg 2 was sunny, as compared with generally rainy or cloudy days during Leg 1.

4.2. Hypoxia and Acidification in the Bottom Water

Hypoxia at the bottom was closely coupled with the phytoplankton blooms in the surface water, suggesting that autochthonous organic matter fuels bottom water DO consumption after settling through the pycnocline (Qian et al., 2018). Based on the coupled analysis of DIC concentrations and the $\delta^{13}C$ of DIC collected during July of 2014, Su et al. (2017) revealed that the remineralization of marine-sourced organic carbon is the dominant process consuming oxygen, and it accounted for 65 ± 16% of the total organic carbon in the Pearl River estuary. Subsequently, Y. Y. Zhao et al. (2020) reported a very strong DIC addition of ~139 ± 21 μmol kg^{-1} and a pH decrease of 0.30 ± 0.04 in hypoxic bottom water in July of 2017, and marine sourced organic carbon contributed 67 ± 18%.

If the remineralization of marine organic matter dominates the oxygen consumption and DIC additions, then the N/P ratio, and the ratio of DIC addition to oxygen consumption should be close to the Redfield ratio (Equation 7, Redfield et al., 1963). The remineralization of organic matter decreases pH as protons are produced.

$$(CH_2O)_{106}(NH_3)_{16}(H_3PO_4) + 138O_2 \rightarrow 106CO_2 + 16NO_3^- + H_2PO_4^- + 17H^+ + 122H_2O \quad (7)$$

As the subsurface and bottom waters were "contaminated" by the DIC produced by remineralization, we use the DIC_{Excess} to quantify DIC accumulation (Xu et al., 2017). The results are shown in Figure 10. In both the bottom and surface waters, AOU and DIC_{Excess} show very similar distribution patterns, which confirms that the bottom water hypoxia was mainly caused by the organic carbon remineralization.

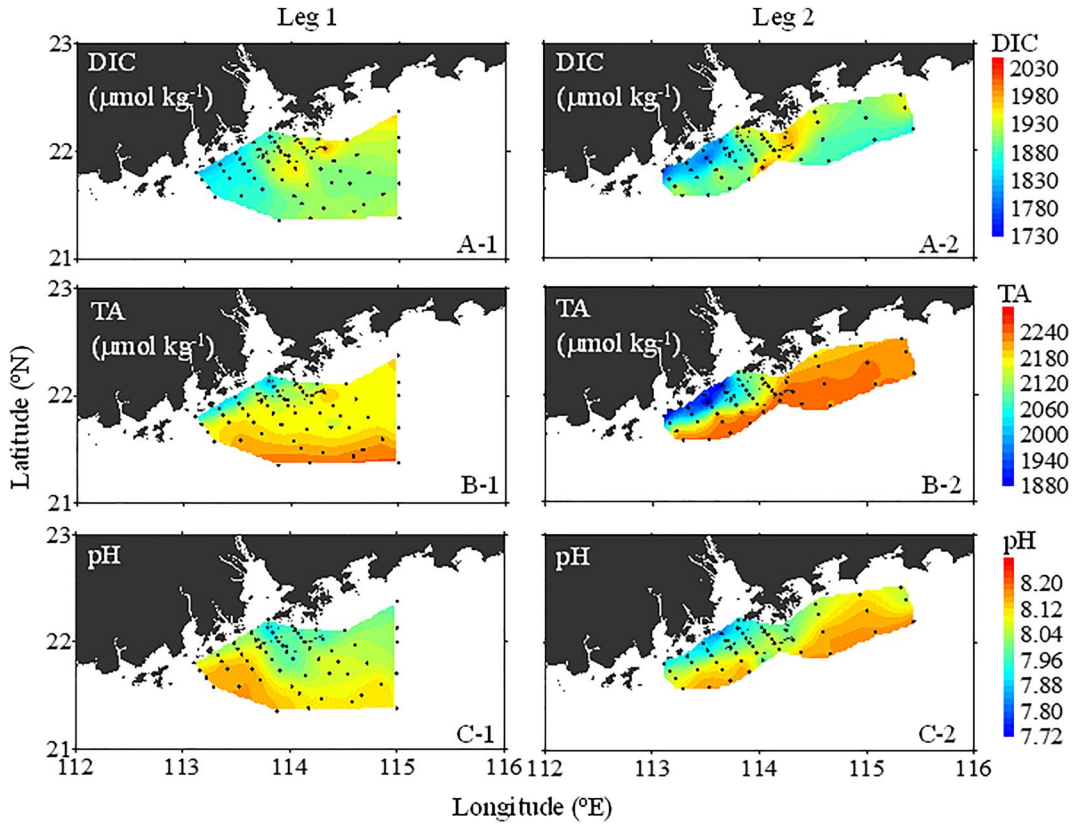

Figure 9. Estimated conservative mixing of dissolved inorganic carbon (DIC), total alkalinity (TA), and pH of the surface. The black dots indicate the sampling stations.

During remineralization, the N+N and SRP show a linear relationship, and the slope of the linear regression is 13.2 (Figure 11). This is slightly lower than the Redfield ratio in the open ocean (16, Redfield et al., 1963), however it is consistent with that of the adjacent northern South China Sea (13.2–14.1, Wong et al., 2007). Additionally, the DIC_{Excess} shows a linear relationship with AOU (m = 0.89), that is slightly greater than the Redfield ratio (m = 0.77), and is approximately equal to the relationships found in the July 2017 and 2018 surveys (m equal to 0.89 and 0.92, respectively, Y. Y. Zhao et al., 2020, 2021). The similarity of the C/O ratio during organic matter remineralization to those of Su et al. (2017) and Y. Y. Zhao et al. (2020) indicates that the decomposition of marine-sourced organic matter is the major driver of oxygen consumption and DIC addition in the bottom water. Additionally, bottom water hypoxia and acidification in the Pearl River estuary/plume occurs almost every summer (2014, 2015, 2017, 2018, Su et al., 2017; Y. Y. Zhao et al., 2020, 2021).

During the two legs, the maximum DIC additions were 132 and 192 μmol kg^{-1}, respectively, and the pH decreases were 0.27 and 0.39 in the hypoxia center. These values are similar to those measured in July 2017 (Y. Y. Zhao et al., 2020). Over the entire surveyed area, average AOUs were 98.5 ± 43.7 and 66.6 ± 30.5 μmol kg^{-1} in the bottom waters during Legs 1 and 2, and the average pH changes were −0.149 ± 0.067 and −0.107 ± 0.057, respectively. Although the area of the acidified bottom water off the Pearl River estuary was smaller than in the northern Gulf of Mexico and the East China Sea (Li et al., 2002; Rabalais et al., 2010), the minimum pH value was similar to those two well-known hypoxic zones.

Table 1
End-Member Values for Simulating the Influence of Upwelling on Surface Water Properties

End-member	Temp. (°C)	Salinity	DIC (μmol kg^{-1})	TA (μmol kg^{-1})
Estuarine water[a]	27.87	20.62	1,860.2	1,978.2
Surface water[b]	29.38	33.63	1,931.8	2,249.9
Bottom water[c]	22.88	34.41	2,113.5	2,274.8

[a]Surface water of the most inshore station of transect A. [b]Surface water of the most offshore station of transect A. [c]Bottom water of the plume center (the buoy station).

Table 2
Comparison of Measured and Calculated Conservative Mixing TA and DIC in Transect F6, the Upwelling Center

	Observed values (μmol kg^{-1})		Conservative mixing values (μmol kg^{-1})	
	TA	DIC	TA	DIC
Leg 1	2,184.4 ± 31.1	1,926.3 ± 40.2	2,183.3 ± 36.8	1,946.0 ± 29.2
Leg 2	2,242.0 ± 11.3	1,979.3 ± 37.4	2,243.2 ± 8.6	1,969.6 ± 34.8

Note. The values are presented as mean ± SD (standard deviations).

4.3. Coupling of Carbon and DO During Remineralization — Reoxygenation and Enhanced Acidification

A comparison of the two legs showed that the hypoxic area was much smaller during Leg 2. During Leg 1, bottom hypoxia occurred at both the estuary mouth and in the western area. However, hypoxia at the estuary mouth disappeared during Leg 2, when it was observed only in the northwestern corner of the study area. We compare the same transects during the two legs (F1 to F6) below.

The mitigation of the hypoxia at the estuary mouth during Leg 2 is mainly attributed to reoxygenation (ventilation) as a result of the downwelling-favorable wind field. During Leg 1, the study area was dominated by

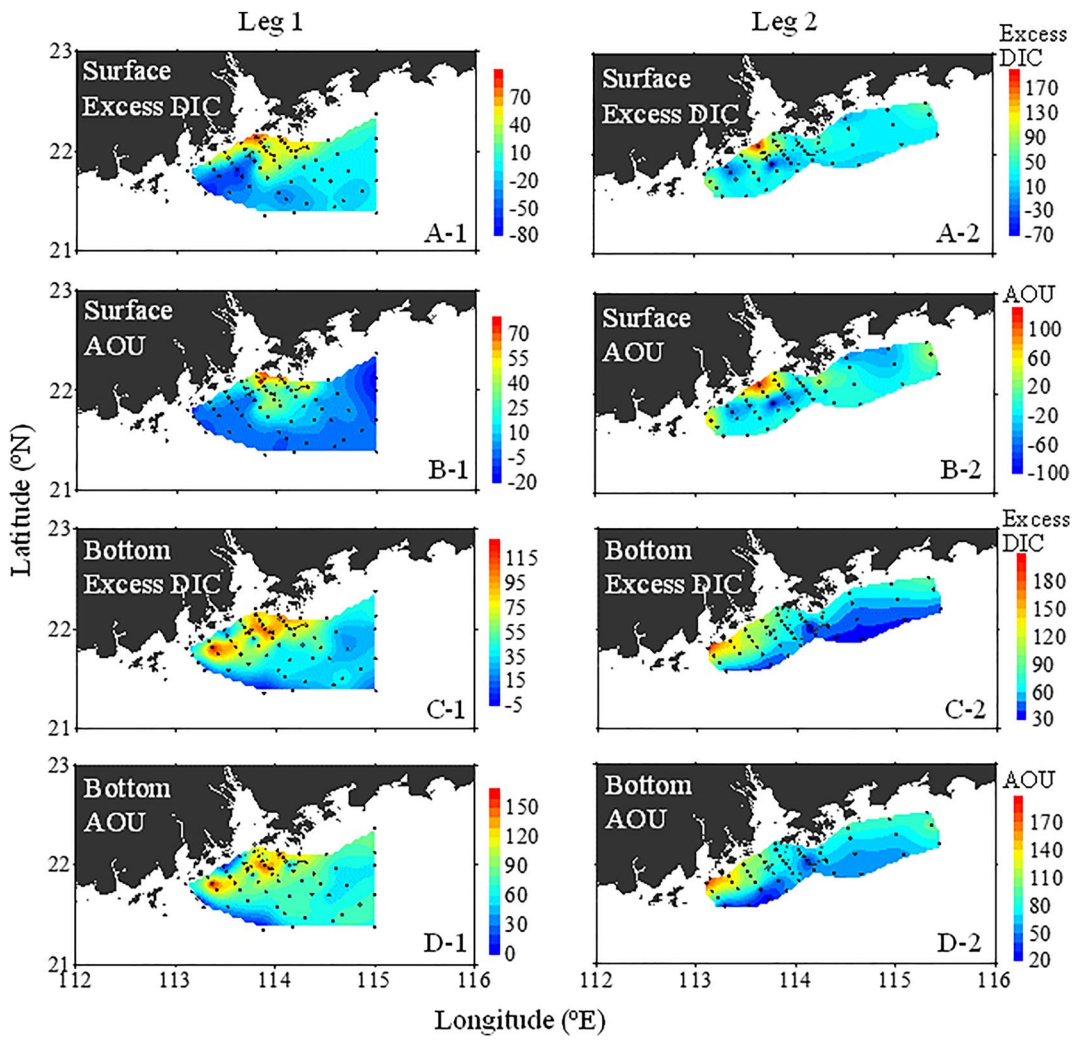

Figure 10. Excess dissolved inorganic carbon (Excess DIC) and apparent oxygen utilization (AOU) in the surface and bottom waters (unit: μmol kg^{-1}). The black dots indicate the sampling stations.

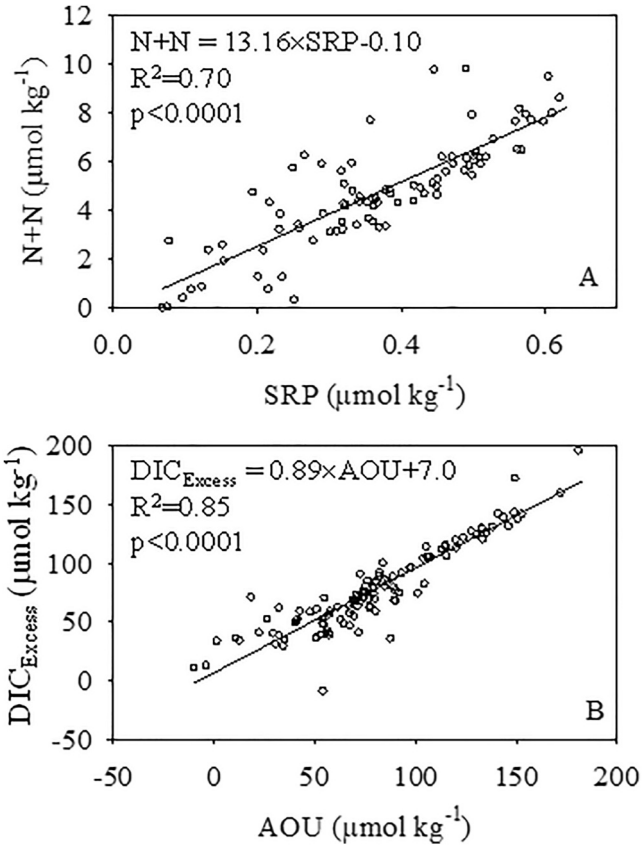

Figure 11. Relationships of nitrate plus nitrite (N+N) and soluble reactive phosphorus (SRP) concentrations (a); excess dissolved inorganic carbon $(DIC)_{Excess}$ and apparent oxygen utilization (AOU) (b) in the bottom water sampled during the two legs of surveys. The solid lines are the linear regressions.

upwelling-favorable winds, which is favorable to form and maintain hypoxia. As a result, bottom hypoxia was prominent during the Leg 1 survey. However, the study area was dominated by downwelling-favorable wind during Leg 2, and depression of the surface water induced ventilation of the bottom water. At the repeated stations (transects A, F5 and F6), average temperature of the water column was 0.34°C higher during Leg 2 than Leg 1 (26.22 ± 1.04°C in Leg 2 vs. 25.88 ± 0.98°C in Leg 1). The average stratification factor was 0.244 ± 0.092 during Leg 1, and it decreased to 0.150 ± 0.096 during Leg 2. The decrease in the stratification factor during Leg 2 is consistent with the enhanced depression of the surface water induced by downwelling-favorable winds.

In the repeated surveyed area (transects F1-F6), the N/P ratio was 13.54 (±1.93) during Leg 1 and 13.51 (±2.04) during Leg 2, and there was no significant difference in the N/P ratios between the two legs (*t* test). DIC_{Excess} and AOU also showed a very good linear relationship during both legs, but the slopes of the linear regressions were different. The C/O ratios during the organic matter degradation were 0.73 (±0.03) during Leg 1 and 0.80 (±0.04) during Leg 2, and were significantly different between the legs (*t* test) (Figure 12). As the equilibration between seawater and atmosphere is ~10 times slower for CO_2 than for O_2 (Zeebe & Wolf-Gladrow, 2003), the amount of CO_2 released should be much smaller than the O_2 supplied from the surface water (and eventually from the atmosphere) during short-term ventilation, resulting in the higher C/O ratio during Leg 2.

pH values also show very good linear relationships with AOU during both legs. This is mainly attributed to the fact that organic matter degradation lowered DO and pH simultaneously (Cai et al., 2011), and is common in areas with large river plumes such as the northern Gulf of Mexico and the East China Sea that experience eutrophication-induced strong remineralization of organic matter (Cai et al., 2011; Jiang et al., 2019). However, the slopes of the linear regressions of the pH-AOU plots were significantly different between the two legs (*t* test): the slope was −0.0016 (±0.0001) during Leg 1 and -0.0019 (±0.0001) during Leg 2. Thus, AOU was lower at the same pH during Leg 2 than during Leg 1. The relatively lower AOU at the same pH during Leg 2 can also be attributed to the difference in the air-water equilibration rate between O_2 and CO_2 during the short-term ventilation. Although we didn't observe the re-establishment of hypoxia after ventilation, it is reasonable to speculate that DIC would be higher and pH lower once hypoxia is re-established after the short-term ventilation. It should be noted that if the ventilation is so strong that the water reaches complete equilibrium with the atmosphere for CO_2, there should be no such differences in the DIC versus AOU and pH versus AOU linear regression slopes before and after ventilation, although this is generally not the case. For DIC, whether the concentration in the bottom water is higher or lower after the ventilation depends on the competition between the ventilation of CO_2 and enhanced remineralization.

Eutrophication-enhanced acidification and hypoxia in the bottom water are usually found along the shallow coasts (Cai et al., 2011; Feely et al., 2018; X. P. Hu et al., 2017). Although episodic perturbation events can relieve hypoxia, they cannot relieve acidification to the same extent. On the contrary, short-term ventilation enhances acidification of bottom water after the re-establishment of the stratification. During episodic ventilation, DO is supplied to the bottom water and CO_2 releases into the atmosphere, but the DIC loss is smaller than the DO supply. When stratification is re-established, the supplied DO increases the pace of organic matter remineralization. Based on these findings, increased episodic ventilation events followed by renewed hypoxia likely increase severe acidification of bottom waters, although other factors (e.g., organic matter supply, water residence time, etc.) also play important roles. Figure 13 is a conceptual model diagram showing this process. This phenomenon may occur in most high productivity marine environments. However, as most of the hypoxia zones are in the shallow coastal areas, which are easily perturbed by storms, this phenomenon is especially likely to occur in coastal

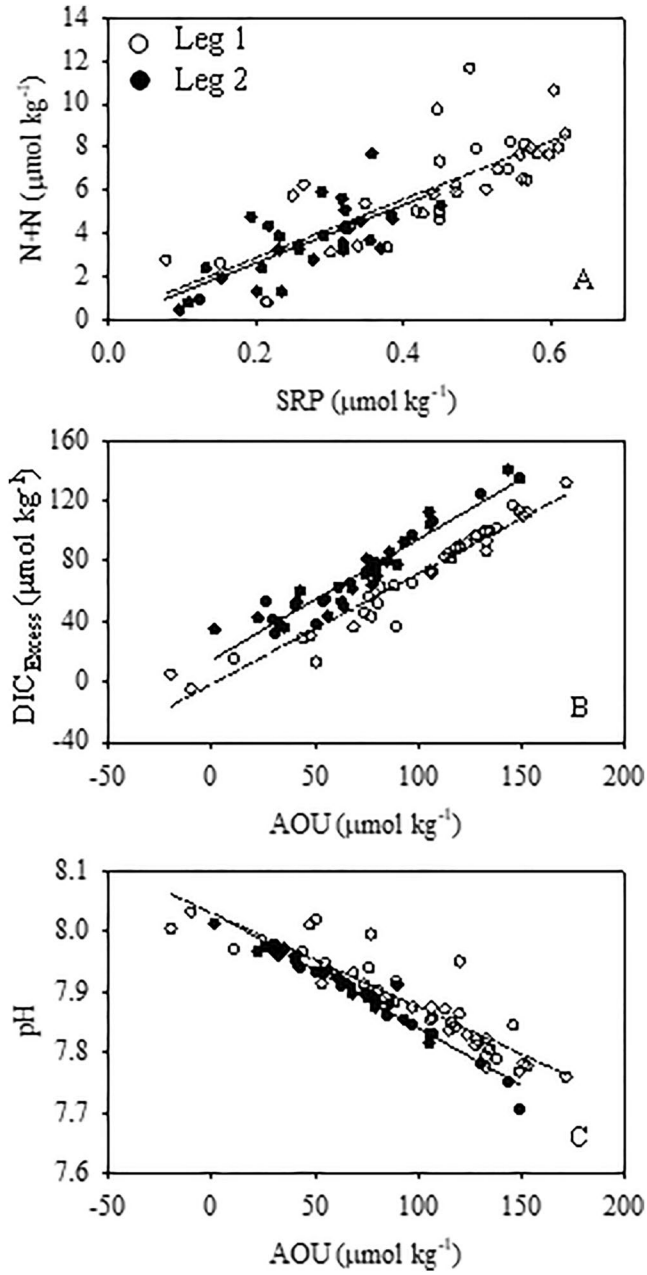

Figure 12. Relationships of nitrate plus nitrite (N+N) and soluble reactive phosphorus (SRP) concentrations (a), excess dissolved inorganic carbon $(DIC)_{Excess}$ and apparent oxygen utilization (AOU) (b), and pH and AOU (c) in the bottom waters of repeated transects F1-F6. The dashed (Leg 1) and solid (Leg 2) lines are the linear regressions (for panel A, the upper line is dashed line and the lower line is solid line). The slopes and intercepts of the linear regressions are expressed as mean (± standard deviation) in the following regression equations:
N+N = 13.5376(±1.9310) × SRP+0.1555(±0.8908), $R^2 = 0.5911$, $p < 0.0001$ (Leg 1)
N+N = 13.5052(±2.0437) × SRP-0.0760(±0.5430), $R^2 = 0.5356$, $p < 0.0001$ (Leg 2)
DIC_{Excess} = 0.7312(±0.0323) × AOU -1.3575 (±3.5031), $R^2 = 0.9301$, $p < 0.0001$ (Leg 1)
DIC_{Excess} = 0.7997(±0.0446) × AOU+14.5980(±3.4140), $R^2 = 0.8985$, $p < 0.0001$ (Leg 2)
pH = −0.0016(±0.0001) × AOU+8.0310(±0.0133), $R^2 = 0.8083$, $p < 0.0001$ (Leg 1)
pH = −0.0019(±0.0001) × AOU+8.0324(±0.0051), $R^2 = 0.9584$, $p < 0.0001$ (Leg 2).

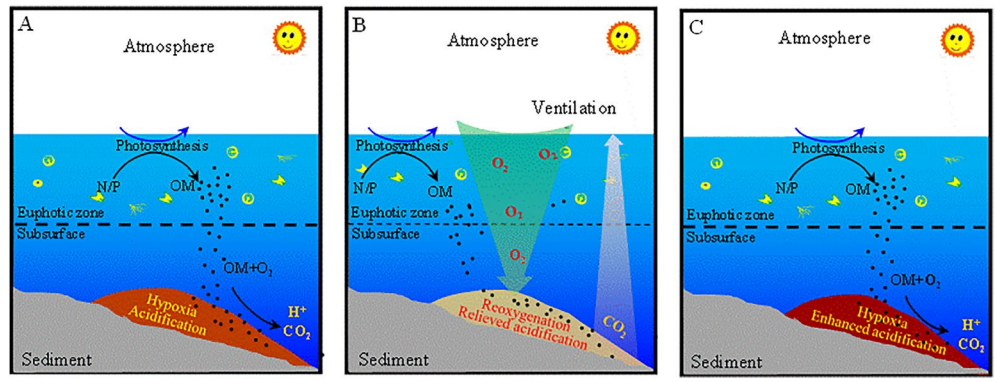

Figure 13. Conceptual model of the enhanced ocean acidification process in bottom water in shallow estuaries or coasts. (a) Status before ventilation; (b) the ventilation process; (c) enhanced acidification after the re-establishment of the stratification following short-term ventilation. N/P indicates nutrients and OM is organic matter. The yellow symbols and black dots denote phytoplankton and particulate OM in the water column, respectively. The thick and thin dashed lines represent strong stratification and weak stratification, respectively.

areas. This enhanced acidification after short-term ventilation has been neglected in ocean acidification studies over the past few decades and should be paid more attention.

5. Concluding Remarks

In July and August of 2015, two legs of a field survey were conducted in the Pearl River plume. Leg 1 was during upwelling-favorable winds while Leg 2 was during donwelling-favorable winds. During both legs, high DIC (>2,000 μmol kg^{-1}), low DO (140–150 μmol kg^{-1}) and acidified (pH 7.7–7.8) surface water was observed at the estuary mouth and the area off Hong Kong as a result of coastal upwelling. During both legs, hypoxia and acidification were observed in the bottom water, covering a larger area during Leg 1 than Leg 2. The stoichiometry of the DIC addition and oxygen consumption suggests that marine-sourced organic matter fuels bottom water DO consumption and induces hypoxia and acidification. However, relationships of DIC addition and pH with oxygen consumption differed between the two legs, with lower AOU at the same levels of DIC addition and pH during Leg 2. This difference can be attributed to short-term ventilation, and the relatively lower CO_2 equilibration rate relative to O_2 during ventilation. As the episodic ventilation supplies oxygen to the bottom water, the pace of remineralization increases, resulting in more acidified water after the re-establishment of hypoxia. This process needs more attention, especially considering the fact that hypoxia and acidified areas occur mostly along the shallow coasts.

Data Availability Statement

The data used in this study (Carbonate system and DO in the Pearl River estuary in summer) are available at the Science Data Bank (https://www.scidb.cn/en/preview?dataSetId=87b4c1ec108b4cc6b720482e7a217772&version=V1) with DOI#:10.57760/sciencedb.09862.

Conflict of Interest

The authors declare no conflicts of interest relevant to this study.

Acknowledgments
The study was supported by the Natural Science Foundation of China (NSFC #41876080), the Strategic Priority Research Program of Chinese Academy of Sciences (Grant XDB42000000), the National Basic Research Program of China through Grant 2015CB954001 (CHOICE-C II), the University Grants Committee of Hong Kong (Grant T21-602/16-R), and the State Key Laboratory of Tropical Oceanography (Grant LTO2102). Faisal Hamzah, Yi Xu, Qi-Pei Shang-Guan, Tao Huang, Peng Cheng, Zhenyu Sun, Jinshun Chen and Junhui Chen are appreciated for their work during the sample collection, measurements and data processing. The authors thank the crews of R/V Haidiao 6 for their assistance during the cruise. Comments by two anonymous reviewers improved the quality of this paper greatly. Richard W. Smith is appreciated for polishing the English.

References

Caballero-Alfonso, A. M., Carstensen, J., & Conley, D. J. (2015). Biogeochemical and environmental drivers of coastal hypoxia. *Journal of Marine Systems*, *141*, 190–199. https://doi.org/10.1016/j.jmarsys.2014.04.008

Cai, W.-J., Dai, M. H., Wang, Y. C., Zhai, W. D., Huang, T., Chen, S. T., et al. (2004). The biogeochemistry of inorganic carbon and nutrients in the Pearl River estuary and the adjacent Northern South China Sea. *Continental Shelf Research*, *24*(12), 1301–1319. https://doi.org/10.1016/j.csr.2004.04.005

Cai, W.-J., Hu, X., Huang, W.-J., Murrell, M. C., Lehrter, J. C., Lohrenz, S. E., et al. (2011). Acidification of subsurface coastal waters enhanced by eutrophication. *Nature Geoscience*, *4*(11), 766–770. https://doi.org/10.1038/ngeo1297

Cao, Z. M., Dai, M. H., Zheng, N., Wang, D. L., Li, Q., Zhai, W. D., et al. (2011). Dynamics of the carbonate system in a large continental shelf system under the influence of both a river plume and coastal upwelling. *Journal of Geophysical Research*, *116*(G02), G02010. https://doi.org/10.1029/2010JG001596

Carpenter, J. H. (1965). The chesapeake bay institute technique for the winkler dissolved oxygen method. *Limnology and Oceanography*, *10*, 141–143. https://doi.org/10.4319/lo.1965.10.1.0141

Carstensen, J., Andersen, J. H., Gustafsson, B. G., & Conley, D. J. (2014). Deoxygenation of the baltic sea during the last century. *Proceedings of the National Academy of Sciences of the United States of America*, *111*(15), 5628–5633. https://doi.org/10.1073/pnas.1323156111

Chou, W. C., Gong, G. C., Cai, W. J., & Tseng, C. M. (2013). Seasonality of CO_2 in coastal oceans altered by increasing anthropogenic nutrient delivery from large rivers: Evidence from the changjiang-east China sea system. *Biogeosciences*, *10*(6), 3889–3899. https://doi.org/10.5194/bg-10-3889-2013

Dai, M. H., Gan, J. P., Han, A. Q., Kung, H. S., Yin, Z. Q., Biahchi, T., et al. (2014). *Physical dynamics and biogeochemistry of the Pearl River plume, biogeochemical dynamics at major river-coastal interface-linkage with global change*. Cambridge University Press. 321–352.

Dai, M. H., Guo, X. H., Zhai, W. D., Yuan, L. Y., Wang, B. W., Wang, L. F., et al. (2006). Oxygen depletion in the upper reach of the Pearl River estuary during a winter drought. *Marine Chemistry*, *102*(1–2), 159–169. https://doi.org/10.1016/j.marchem.2005.09.020

Dickson, A. G. (1990). Thermodynamics of the dissociation of boric acid in synthetic sea water from 273.15 to 318.15 K. *Deep-Sea Research, Part A: Oceanographic Research Papers*, *37*(5), 755–766. https://doi.org/10.1016/0198-0149(90)90004-f

Dickson, A. G., Sabine, C. L., & Christian, J. R. (2007). *Guide to best practices for ocean CO2 measurement* (Vol. 3). PICES Special Publication.

Dong, X., Huang, H., Zheng, N., Pan, A., Wang, S., Huo, C., et al. (2017). Acidification mediated by a river plume and coastal upwelling on a fringing reef at the east coast of Hainan Island, Northern South China Sea. *Journal of Geophysical Research-Oceans*, *122*(9), 7521–7536. https://doi.org/10.1002/2017jc013228

Feely, R. A., Okazaki, R. R., Cai, W.-J., Bednarsek, N., Alin, S. R., Byrne, R. H., & Fassbender, A. (2018). The combined effects of acidification and hypoxia on pH and aragonite saturation in the coastal waters of the California current ecosystem and the northern Gulf of Mexico. *Continental Shelf Research*, *152*, 50–60. https://doi.org/10.1016/j.csr.2017.11.002

Feely, R. A., Sabine, C. L., Hernandez-Ayon, J. M., Ianson, D., & Hales, B. (2008). Evidence for upwelling of corrosive "acidified" water onto the continental shelf. *Science*, *320*(5882), 1490–1492. https://doi.org/10.1126/science.1155676

Fennel, K., & Testa, J. M. (2019). Biogeochemical controls on coastal hypoxia. *Annual Review of Marine Science*, *11*, 105–130. https://doi.org/10.1146/annurev-marine-010318-095138

Gan, J. P., Cheung, A., Guo, X. G., & Li, L. (2009). Intensified upwelling over a widened shelf in the northeastern South China Sea. *Journal of Geophysical Research*, *114*(C09), C09019. https://doi.org/10.1029/2007jc004660

Garcia, H. E., & Gordon, L. I. (1992). Oxygen solubility in seawater-better fitting equations. *Limnology and Oceanography*, *37*(6), 1307–1312. https://doi.org/10.4319/lo.1992.37.6.1307

Grantham, B. A., Chan, F., Nielsen, K. J., Fox, D. S., Barth, J. A., Huyer, A., et al. (2004). Upwelling-driven nearshore hypoxia signals ecosystem and oceanographic changes in the northeast Pacific. *Nature*, *429*(6993), 749–754. https://doi.org/10.1038/nature02605

Guo, X. H., Dai, M. H., Zhai, W. D., Cai, W. J., & Chen, B. S. (2009). CO_2 flux and seasonal variability in a large subtropical estuarine system, the Pearl River estuary, China. *Journal of Geophysical Research*, *114*, G03013. https://doi.org/10.1029/2008jg000905

Han, A. Q., Dai, M. H., Kao, S.-J., Gan, J. P., Li, Q., Wang, L. F., et al. (2012). Nutrient dynamics and biological consumption in a large continental shelf system under the influence of both a river plume and costal upwelling. *Limnology and Oceanography*, *57*(2), 486–502. https://doi.org/10.4319/lo.2012.57.2.0486

Hansen, D. V., & Rattray, M. J. (1966). New dimensions in estuary classification. *Limnology and Oceanography*, *11*(3), 319–326. https://doi.org/10.4319/lo.1966.11.3.0319

Hansen, H. P., & Koroleff, F. (1999). Determination of nutrients. In K. Grasshoff, K. Kremling, & M. Ehrhardt (Eds.), (Eds.,) *Methods of seawater analysis* (pp. 159–228). Toronto Wiley-VCH.

Hu, J. Y., Kawamura, H., Hong, H., & Qi, Y. (2000). A review on the currents in the south China sea: Seasonal circulation, south China sea current and kuroshio intrusion. *Journal of Oceanography*, *56*, 607–624. https://doi.org/10.1023/a:1011117531252

Hu, X. P., Li, Q., Huang, W.-J., Chen, B., Cai, W.-J., Rabalais, N. N., & Turner, E. R. (2017). Effects of eutrophication and benthic respiration on water column carbonate chemistry in a traditional hypoxic zone in the Northern Gulf of Mexico. *Marine Chemistry*, *194*, 33–42. https://doi.org/10.1016/j.marchem.2017.04.004

Jiang, Z.-P., Cai, W.-J., Chen, B., Wang, K., Han, C., Roberts, B. J., et al. (2019). Physical and biogeochemical controls on pH dynamics in the northern Gulf of Mexico during summer hypoxia. *Journal of Geophysical Research: Oceans*, *124*(8), 5979–5998. https://doi.org/10.1029/2019jc015140

Jing, Z. Y., Qi, Y., Du, Y., Zhang, S., & Xie, L. (2015). Summer upwelling and thermal fronts in the northwestern South China Sea: Observational analysis of two mesoscale mapping surveys. *Journal of Geophysical Research: Oceans*, *120*(3), 1993–2006. https://doi.org/10.1002/2014jc010601

Jutras, M., Dufour, C. O., Mucci, A., Cyr, F., & Gilbert, D. (2020). Temporal changes in the causes of the observed oxygen decline in the St. Lawrence estuary. *Journal of Geophysical Research: Oceans*, *125*(12), e2020JC016577. https://doi.org/10.1029/2020jc016577

Labasque, T., Chaumery, C., Aminot, A., & Kergoat, G. (2004). Spectrophotometric winkler determination of dissolved oxygen: Re-examination of critical factors and reliability. *Marine Chemistry*, *88*(1–2), 53–60. https://doi.org/10.1016/j.marchem.2004.03.004

Li, D. J., Zhang, J., Huang, D. J., Wu, Y., & Liang, J. (2002). Oxygen depletion off the changjiang (yangtze river) estuary. *Science in China — Series D: Earth Sciences*, *45*(12), 1137–1146. https://doi.org/10.1360/02yd9110

Lin, H. Y., Liu, S., & Han, W. Y. (2001). Potential trigger CTB from seasonal bottom water hypoxia in the Pearl River estuary. *Journal of Zhejiang Ocean University*, *21*, 25–29. (In Chinsese with English abstract).

Lin, P. G., Cheng, P., Gan, J. P., & Hu, J. Y. (2016). Dynamics of wind-driven upwelling off the northeastern coast of Hainan Island. *Journal of Geophysical Research: Oceans*, *121*(2), 1160–1173. https://doi.org/10.1002/2015jc011000

Liu, Z. Q., Gan, J. P., & Wu, X. Y. (2018). Coupled summer circulation and dynamics between a bay and the adjacent shelf around Hong Kong: Observational and modeling studies. *Journal of Geophysical Research: Oceans*, *123*(9), 6463–6480. https://doi.org/10.1029/2018jc013830

Liu, Z. Q., Zu, T. T., & Gan, J. P. (2020). Dynamics of cross-shelf water exchanges off Pearl River estuary in summer. *Progress in Oceanography*, *189*, 102465. https://doi.org/10.1016/j.pocean.2020.102465

Millero, F. J., Graham, T. B., Huang, F., Bustos-Serrano, H., & Pierrot, D. (2006). Dissociation constants of carbonic acid in seawater as a function of salinity and temperature. *Marine Chemistry*, *100*(1–2), 80–94. https://doi.org/10.1016/j.marchem.2005.12.001

Monteiro, P. M. S., Van der Plas, A., Mohrholz, V., Mabille, E., Pascall, A., & Joubert, W. (2006). Variability of natural hypoxia and methane in a coastal upwelling system: Oceanic physics or shelf biology? *Geophysical Research Letters*, *33*(16), L16614. https://doi.org/10.1029/2006gl026234

Pierrot, D., Lewis, E., & Wallace, W. R. (2006). MS excel program developed for CO2 system calculations. In *ORNL/CDIAC-105a*. Carbon Dioxide Information Analysis Center, Oak Ridge National Laboratory, U.S. Department of Energy.

Qian, W., Gan, J. P., Liu, J. W., He, B. Y., Lu, Z. M., Guo, X. H., et al. (2018). Current status of emerging hypoxia in a eutrophic estuary: The lower reach of the Pearl River estuary, China. *Estuarine, Coastal and Shelf Science*, *205*, 58–67. https://doi.org/10.1016/j.ecss.2018.03.004

Rabalais, N. N., Diaz, R. J., Levin, L. A., Turner, R. E., Gilbert, D., & Zhang, J. (2010). Dynamics and distribution of natural and human-caused hypoxia. *Biogeosciences*, *7*(2), 585–619. https://doi.org/10.5194/bg-7-585-2010

Rabalais, N. N., Turner, R. E., & Wiseman, W. J. (2002). Gulf of Mexico hypoxia, aka "The dead zone". *Annual Review of Ecology and Systematics*, *33*, 235–263. https://doi.org/10.1146/annurev.ecolsys.33.010802.150513

Redfield, A. C., Ketchum, B. H., & Richards, B. H. (1963). *The influence of organisms on the composition of seawater*. The Sea. In M. N. Hill (Ed.), (Ed.,) Interscience Publisher., 2, 26–77.

Su, J. Z., Dai, M. H., He, B. Y., Wang, L. F., Gan, J. P., Guo, X. H., et al. (2017). Tracing the origin of the oxygen-consuming organic matter in the hypoxic zone in a large eutrophic estuary: The lower reach of the Pearl River estuary, China. *Biogeosciences*, *14*(18), 4085–4099. https://doi.org/10.5194/bg-14-4085-2017

Wang, H. J., Dai, M. H., Liu, J. W., Kao, S.-J., Zhang, C., Cai, W.-J., et al. (2016). Eutrophication-driven hypoxia in the East China sea off the changjiang estuary. *Environmental Science and Technology*, *50*(5), 2255–2263. https://doi.org/10.1021/acs.est.5b06211

Weiss, R. F. (1974). Carbon dioxide in water and seawater: The solubility of a non-ideal gas. *Marine Chemistry*, *2*, 203–215. https://doi.org/10.1016/0304-4203(74)90015-2

Wong, G. T. F., Tseng, C.-M., Wen, L.-S., & Chung, S.-W. (2007). Nutrient dynamics and N-anomaly at the SEATS station. *Deep Sea Research Part II: Topical Studies in Oceanography*, *54*(14–15), 1528–1545. https://doi.org/10.1016/j.dsr2.2007.05.011

Xu, Y.-Y., Pierrot, D., & Cai, W.-J. (2017). Ocean carbonate system computation for anoxic waters using an updated CO2SYS program. *Marine Chemistry*, *195*, 90–93. https://doi.org/10.1016/j.marchem.2017.07.002

Yin, K. D., Lin, Z. F., & Ke, Z. Y. (2004). Temporal and spatial distribution of dissolved oxygen in the Pearl River estuary and adjacent coastal waters. *Continental Shelf Research*, *24*(16), 1935–1948. https://doi.org/10.1016/j.csr.2004.06.017

Zeebe, R. E., & Wolf-Gladrow, D. (2003). *CO_2 in seawater: Equilibrium, kinetics, isotopes*. Elsevier.

Zhai, W. D., Dai, M. H., Cai, W.-J., Wang, Y. C., & Wang, Z. H. (2005). High partial pressure of CO_2 and its maintaining mechanism in a subtropical estuary: The Pearl River estuary, China. *Marine Chemistry*, *93*(1), 21–32. https://doi.org/10.1016/j.marchem.2004.07.003

Zhao, H. T. (1990). *Evolution of the Pearl River estuary* (pp. 357). Ocean Press. (in Chinese).

Zhao, Y. Y., Liu, J., Uthaipan, K., Song, X., Xu, Y., He, B. Y., et al. (2020). Dynamics of inorganic carbon and pH in a large subtropical continental shelf system: Interaction between eutrophication, hypoxia and ocean acidification. *Limnology and Oceanography*, *65*, 1359–1379. https://doi.org/10.1002/lno.11393

Zhao, Y. Y., Uthaipan, K., Lu, Z. M., Li, Y., Liu, J., Liu, H. B., et al. (2021). Destruction and reinstatement of coastal hypoxia in the south China sea off the Pearl River estuary. *Biogeosciences*, *18*, 2755–2775. https://doi.org/10.5194/bg-18-2755-2021

Zu, T. T., & Gan, J. P. (2015). A numerical study of coupled estuary-shelf circulation around the Pearl River estuary during summer: Responses to variable winds, tides and river discharge. *Deep Sea Research Part II: Topical Studies in Oceanography*, *117*, 53–64. https://doi.org/10.1016/j.dsr2.2013.12.010